Meridional circulation in the western coastal zone:

I. Variability of off-shore thermocline depth and western boundary current transport on interannual and decadal time scales

Rui Xin Huang[*+] & Qinyan Liu[+$]

[*] Woods Hole Oceanographic Institution, Woods Hole, MA 02543, USA

[+] South China Sea Institute of Oceanology, Chinese Academy of Sciences, Guangzhou, China

January 29, 2010

Will be submitted to *J. Phys. Oceanography*

[$] Corresponding author: Qinyan Liu, South China Sea Institute of Oceanology, Chinese Academy of Sciences, Guangzhou, China, qyliu66@scsio.ac.cn

Abstract

Based on the framework of a reduced gravity model for the wind-driven gyres in the ocean interior, the western boundary current transport and the meridional pressure gradient along the outer edge of the western coastal regime of the wind-driven gyre are examined. Since the first baroclinic Rossby waves take several years to cross the basin, the model is valid for interannual/decadal time scale only. It is shown that this meridional pressure gradient can be calculated as the meridional gradient of the zonal wind stress integrated from the western boundary to the eastern boundary, without the contribution from the meridional wind stress and the delay term associated with the propagation of Rossby waves. On the other hand, the western boundary current transport consists of contributions due to zonal wind stress and the delayed Ekman pumping integration. The exclusion/inclusion of the Rossby wave delay term gives rise to the substantial difference in the variability of these two terms and their role in regulating the coastal circulation adjacent to the western boundary of the wind-driven gyre.

1. Introduction

The circulation in a basin is commonly studied in terms of interior circulation of basin scale and the coastal circulation of a rather narrow length scale in the off-shore direction. The interaction between the open ocean and the coastal ocean involves complicated phenomena. In a review article by Brink (1998) a major dynamical barrier for the interaction between the open ocean and the coastal ocean was postulated. Although Brink also pointed out that this barrier can be overcome by friction, nonlinearity and external force, the way to break this barrier remains unclear.

In fact, most previous studies of coastal circulation have been focused on the relatively narrow coastal zone, without paying much attention to the possible interaction between the open ocean and the coastal zone. Due to the limitation of computer power, many coastal models have been formulated, based upon the so-called open boundary condition. The common practice was specifying the circulation condition along the outer edge of the coastal model zone with the climatological state obtained from either observations or numerical models.

One of the major shortcomings of such a practice is that changes of the circulation in the basin interior cannot be accurately reflected in the coastal model. Recent studies indicated that information from the open ocean does affect the coastal circulation on low frequency time scale. The first example is the study by Hong et al. (2000) demonstrating a close connection between the interannual variability in coastal sea level along the eastern United States and the westward baroclinic Rossby waves due to changes in winds over the open Atlantic Ocean. The second example is the meridional currents in the

coastal zone flowing in the direction opposite to the local wind stress. One of such cases is the flow in the Taiwan Strait. Although wind stress in winter season is southward, current in the strait flows northward, against the local wind stress. Similar phenomena related to a coastal current flowing against local wind stress remained unsettled for a long time. Yang (2007) went through a careful dynamical analysis and pointed out that such current is primarily due to the pressure gradient force associated with western boundary current, such as the Kuroshio in the North Pacific Ocean.

In this study, we will refine Yang's analysis in light of the boundary layer theory (Schlichting, 1979) widely used in fluid dynamics. The ocean is separated into three parts, the interior flow, the western boundary layer current, and the costal current over the continental shelf, Fig. 1. For the interior regime, flow is controlled by a balance of geostrophy, Coriolis force and wind stress; while other frictional forces can be neglected. The western boundary current is subject to the semi-geostrophy: the Coriolis force associated with the downstream velocity is balanced by the cross-stream pressure gradient, and the wind stress force is negligible; while the Coriolis force associated with the cross-stream velocity is balanced by down-stream pressure gradient, wind stress, and friction.

The coastal circulation in this framework is treated as a thin boundary layer attached to the interior solution and the western boundary current, Fig. 1. As in many applications of boundary layer theory, the along-stream pressure gradient is primarily set up by the circulation outside the coastal zone. Since the coastal boundary is relatively thin and the associated total volumetric transport is small compared with the interior

circulation, the along-stream pressure gradient can be considered approximately constant in the cross-stream direction. Therefore, the coastal circulation in the along-shore direction is the outcome of the competition of the along-shore pressure gradient set up by basin-scale circulation and the local wind stress.

This study is organized as follows. The theoretical framework is built up in Section 2. First, we demonstrate that to a large degree, the meridional current in the western coastal zone is subject to a meridional pressure gradient set up by the basin-scale wind-driven circulation. Second, as wind stress in the basin interior changes with time, this pressure gradient also changes. Thus, coastal circulation is subject to the decadal variability of wind stress in the basin interior, and the study of coastal circulation cannot be carried in isolation. In Section 3, as a simple test, this theory is then applied to the western edge of the open North Pacific Ocean, where the thermocline depth predicted by the simple wind stress calculation and diagnosed from the SODA data is compared. We finally conclude in Section 4.

2. Model formulation

A. Circulation in the basin interior

In the basin interior the circulation can be described in terms of a reduced gravity model. For a more comprehensive discussion of the reduced gravity model and its application to wind-driven gyres in the ocean, the reader is referred to Huang (2010). For the present case, the basic equations are

$$-fv = -g'\frac{\partial h}{\partial x} + \tau^x / \rho_0 H \,, \tag{1}$$

$$fu = -g'\frac{\partial h}{\partial y} + \tau^y / \rho_0 H \,, \tag{2}$$

$$\frac{\partial h}{\partial t} + H\left(\frac{\partial u}{\partial x} + \frac{\partial v}{\partial y}\right) = 0 \,. \tag{3}$$

where f is the Coriolis parameter, (u,v) are the horizontal velocity, g' is the reduced gravity, h is the layer thickness and H is the mean layer thickness, $\left(\tau^x, \tau^y\right)$ are the zonal and meridional wind stress, and ρ_0 is the constant reference density. Note that for circulation on time scale of monthly, annual or even longer, the time dependent terms in the horizontal momentum equations are much smaller than the Coriolis terms, and thus negligible; however, it is not negligible in the continuity equation.

The basic assumption of the reduced gravity model is that the lower layer is much thicker than the upper layer, so that velocity in the lower layer is much smaller than that in the upper layer. For an ocean forced by time-varying wind, the barotropic Rossby waves set up the all-depth circulation. With the first baroclinic waves passing through a station, the deep current is reset to nearly zero. Thus, the reduced gravity model is valid for time scales comparable to or longer than the cross-basin time scale of the first baroclinic waves. For the latitudinal band of 15^o-30^oN, the corresponding time is about 4 to 15 years (2-7 years) for the Pacific (Atlantic) basin; thus, the results obtained from a reduced gravity model is not valid for time scale much shorter. For example, it is not valid for monthly mean circulation. On the other hand, for circulation on interannual to

decadal time scales, the reduced gravity model should provide quite useful results. Of course, whether results obtained from a model based on such an approximation are usable for our understating of the oceanic circulation will be judged from analysis of data obtained from the more sophisticated model, and this will be discussed in detail in Part II of this study (Liu and Huang, manuscript).

Cross-differentiating (1, 2) and subtracting lead to the vorticity equation

$$f\left(\frac{\partial u}{\partial x}+\frac{\partial v}{\partial y}\right)+\beta v=\frac{1}{\rho_0 H}\left(\frac{\partial \tau^y}{\partial x}-\frac{\partial \tau^x}{\partial y}\right). \tag{4}$$

Substituting (4) into (3) and using (1) lead to

$$\frac{\partial h}{\partial t}-C(y)\frac{\partial h}{\partial x}=-w_e>0, C(y)=\frac{\beta g' H}{f}, w_e=\frac{1}{f\rho_0}\left(\frac{\partial \tau^y}{\partial x}-\frac{\partial \tau^x}{\partial y}+\frac{\beta\tau^x}{f}\right)<0, \tag{5}$$

where $C(y)$ is the speed of long Rossby waves, and w_e is the Ekman pumping velocity.

Note that one can also formulate a non-linear version of the problem, using

$$-fhv=-g'h\frac{\partial h}{\partial x}+\tau^x/\rho_0, \tag{1'}$$

$$fhu=-g'h\frac{\partial h}{\partial y}+\tau^y/\rho_0, \tag{2'}$$

$$\frac{\partial h}{\partial t}+\left(\frac{\partial hu}{\partial x}+\frac{\partial hv}{\partial y}\right)=0. \tag{3'}$$

However, the wave speed in the equation corresponding to Eq. (5) will be $C(y)=\frac{\beta g' h}{f^2}$.

The wave speed depends on the amplitude of the layer thickness. Such a nonlinear wave equation involves complicated phenomena which are beyond the scope of this study; thus, we will use the linear version of the model discussed above.

In order to solve the partial differential equation (5) we introduce the new variables,

$$\xi = t + x/C(y), \eta = t - x/C(y), \text{ or, } t=(\xi+\eta)/2, x = C(\xi-\eta)/2. \quad (6)$$

Equation (5) is reduced to

$$\frac{\partial h}{\partial \eta} = -\frac{1}{2} w_e\left(C(y)\frac{\xi-\eta}{2}, y, \frac{\xi+\eta}{2}\right). \quad (7)$$

Integrating (7) along a characteristic $\xi = const.$ leads to

$$h = h(\xi, y, \eta_e) - \frac{1}{2}\int_{\eta_e}^{\eta} w_e(\xi, y, \eta)\, d\eta. \quad (8)$$

Replacing the new coordinates with the old coordinates, i.e., $(\xi,\eta)\to(x,t)$, we have $d\eta = -2dx/C(y)$. Since the integration is along $\xi = const.$, $\xi = t + x/C(y) = const.$ is treated as fixed. Therefore, variable *t* is replaced by $t \to \xi - x'/C(y) = t + (x-x')/C(y)$. Eq. (8) is reduced to

$$h = h\left(x_e, y, t + \frac{x-x_e}{C(y)}\right) - \frac{f^2}{\beta g' H}\int_x^{x_e} w_e\left(x', y, t + \frac{x-x'}{C(y)}\right) dx'. \quad (9)$$

The second term on the right-hand side of (9) is called the time delay term associated with Rossby waves, which has been discussed in many previous studies, e.g., Willebrand et al. (1980) and Qiu (2002). This equation can be used to calculate the delayed response of layer thickness and meridional volume transport in the basin interior. In particular, at the outer edge of the western boundary current, (this can be denoted as $x_w = 0^+$, where the superscript + indicates the eastern outer edge of the very thin boundary layer), the layer thickness is

$$h_I(0,y,t) = h\left(x_e, y, t - \frac{x_e}{C(y)}\right) - \frac{f^2}{\beta g' H}\int_0^{x_e} w_e\left(x', y, t - \frac{x'}{C(y)}\right)dx' \qquad (10)$$

B. Pressure gradient along the western edge of the open ocean

Along the western boundary, the narrow western boundary current satisfies the semi-geostrophy, so that the Coriolis force associated with the downstream velocity is balanced by the cross-stream pressure gradient force; thus, Eq. (1) is reduced to

$$-fv = -g'\frac{\partial h}{\partial x}. \qquad (11)$$

Since the net meridional volume transport in a closed basin must be zero, the equatorward volume transport of the interior flow at the outer edge of the western boundary should equal to the poleward flux of the western boundary current, and we use ψ_I to denote this flux. Multiplying the mean layer thickness H and integrating (11) across the narrow boundary current, we obtain a relation between the transport of the narrow western boundary current and the layer thickness difference across the stream

$$\psi_I = \frac{g'H}{f}\left(h_I - h_W\right), \tag{12}$$

where h_I and h_W are the layer thickness for the interior solution on the outer edge of the western boundary and layer thickness along the "western wall". In deriving this relation, we have used the default boundary condition that the western boundary is a line of zero streamfunction. This implies that the branching of the western boundary current into the shelf transport is much smaller than that of the western boundary current, and thus it can be neglected. This equation can be rewritten as

$$h_W = h_I - \frac{f}{g'H}\psi_I\,. \tag{13}$$

The interior streamfunction at the outer edge of the western boundary can be obtained by integrating Eq. (1) across the basin interior, i.e.,

$$\psi_I = \int_{x_e}^{0} Hv\,dx = \frac{g'H}{f}\left[h_I\left(0,y,t\right) - h_e(x_e,y,t)\right] - \frac{1}{f\rho_0}\int_{x_e}^{0}\tau^x\left(x',y,t\right)dx', \tag{14}$$

where $h_e = h_e\left(x_e,y,t\right)$ is the layer thickness along the eastern boundary at the current time t. On the other hand, if we apply Eq. (9) to calculate the layer thickness along the western wall, the first term on the right-hand side of Eq. (9) represents the corresponding layer thickness along the eastern boundary at the eralier time, $t - x_e / C\left(y\right) < t$. In general, layer thickness along the eastern boundary also varies with time; thus, these two terms are different. However, for simplicity we will omit this difference, i.e., it will be

assumed that layer thickness along the eastern boundary remain a fixed value all the time. Substituting (9) into (13) leads to

$$\psi_I = -\frac{f}{\beta}\int_0^{x_e} w_e\left(x', y, t - \frac{x'}{C(y)}\right)dx' + \frac{1}{f\rho_0}\int_0^{x_e}\tau^x dx + \frac{g'H}{f}\left[h_e\left(x_e, y, t - \frac{x_e}{C(y)}\right) - h_e(x_e, y, t)\right] \tag{15}$$

Substituting (14) into (13) leads to

$$h_W(0, y, t) = h_e(x_e, y, t) - \frac{1}{\rho_0 g'H}\int_0^{x_e}\tau^x(x', y, t)\,dx' . \tag{16}$$

This equation can be interpreted as follows. In a quasi-steady state, the equatorward volumetric flux in the ocean interior, including the ageostrophic Ekman flux V_E and the geostrophic flux V_I in the subsurface layer, has to be transported poleward through the western boundary zone ; thus, the total volumetric transport in the western boundary layer is $V_W = -(V_I + V_E)$, Fig. 2. Let us conceptually separate the western boundary current into two branches. The first branch contains the volumetric flux V_I which balances the equatorward flow in the ocean interior. Therefore, at the western edge of this branch of the western boundary current the depth of the main thermocline is exactly the same as that along the eastern boundary $h_{W,1} = h_e$. The second branch should carry the volumetric flux associated with the surface Ekman layer in the ocean interior, i.e., V_E ; thus, the depth of the main thermocline at the western edge of this second branch should satisfy Eq. (16).

As shown in Fig. 1, the thermocline thickness along the edge of the "western wall", h_W, obtained from the basin-scale circulation can provide a large-scale pressure gradient force for the relatively narrow coastal circulation in the marginal sea adjacent to the western boundary of the basin.

In the following analysis, we will assume that the layer thickness along the eastern boundary is constant, i.e., it is invariant with time and latitude. Thus, omitting the last two terms within the square brackets, Eq. (15) is reduced to the following form

$$\psi_I = -\frac{f}{\beta}\int_0^{x_e} w_e\left(x', y, t - \frac{x'}{C(y)}\right)dx' + \frac{1}{f\rho_0}\int_0^{x_e}\tau^x dx\,. \qquad (15')$$

Within the framework of a reduced gravity model, the corresponding meridional pressure gradient force along the western wall is

$$-\frac{1}{\rho_0}\frac{\partial p}{\partial y} = -\frac{1}{\rho_0 H}\frac{\partial P}{\partial y} = g'\frac{\partial h_w}{\partial y} = \frac{1}{\rho_0 H}\int_0^{x_e}\frac{\partial \tau^x}{\partial y}dx, \text{ or } \frac{\partial P}{\partial y} = -\int_0^{x_e}\frac{\partial \tau^x}{\partial y}dx\,. \qquad (17)$$

Therefore, under our basic assumptions, i.e., for time scale of annual or longer, the meridional pressure gradient at the outer edge of the coastal ocean is set up by the meridional gradient of the zonal integration of the zonal wind stress. It is interesting to note that under our assumptions, the meridional wind stress in the basin interior made no contribution to the meridional pressure gradient along the western wall.

We notice that the interior solution is subjected to the delay of baroclinic Rossby waves, as depicted by Eqs. (9) and (10); thus, the layer thickness along the outer edge of the western boundary is set up by the delayed Rossby waves. However, the pressure

gradient along the western wall is not affected by this delay, i.e., this pressure reflects contributions from wind stress in different parts of the basin interior at the same time. On the other hand, the transport of the western boundary current is controlled by both the delayed Rossby wave and the pressure gradient force due to the "instantaneous" zonal wind stress. As a result, western boundary transport reflects wind stress curl contribution at different time for different part of the basin. Therefore, for the case subject to wind force with interannual/decadal variability, these three physical quantities should respond in quite different ways.

Note that our discussion above applies to both the subtropical and subpolar basin. A numerical example of the steady circulation in a two gyre basin, based on the corresponding equations in spherical coordinate, is shown in Fig. 3. The model is set up for a subtropical-subpolar basin [15°N, 60°N]. A simple wind stress profile is used $\tau^x = \tau_0 \cos\left(2\pi \frac{y - y_s}{y_n - y_s}\right), y_s = 15^o N, y_n = 60^o N$. To avoid outcropping of the lower layer in the subpolar basin, we selected the following parameters: $\tau_0 = -0.03 N/m^2$, $h_e = H = 600m$, $g' = 0.05 m/s^2$, $x_e - x_w = 40^o$. Based on the assumption that the lower layer is stagnant, the equivalent surface elevation perturbation is calculated as $\eta = (h - H) g'/g$, subject to the constraint that the mean surface elevation is set to zero.

For the basin scale circulation, there are the westerlies at middle latitudes, thus, the pressure gradient force along the western wall set up by the basin-scale circulation imposes a northward pressure gradient force in the subtropical gyre interior. On the other

hand, in the subpolar basin, the meridional pressure gradient force along the western wall is equatorward, Fig. 3. As will be discussed in Part II, scaling analysis indicates that the meridional pressure gradient set up by basin scale circulation is one order of magnitude larger than the local meridional wind stress imposed on the coastal zone. As a result, meridional current in the coastal zone is primarily controlled by this meridional pressure gradient force; however, the detailed discussion will be presented in part II.

C. Pressure gradient, thermocline depth and transport

The relation between the thermocline depth, transport of the western boundary current and the meridional pressure gradient can be best illustrated through the following simple example. The model ocean is a subtropical basin between 15N and 40N, with a width of 60^o (mimicking the North Atlantic Ocean) and 120^o (mimicking the North Pacific Ocean).

To demonstrate the basic idea, we use wind stress in the following two forms:

$$\text{Case A: } \tau_A^x = -\tau_0 \cos\frac{\pi(\theta-\theta_s)}{\theta_n-\theta_s} - \Delta\tau\frac{\theta-\theta_s}{\theta_n-\theta_s}\cos\frac{2\pi t}{T} \tag{18a}$$

$$\text{Case B: } \tau_B^x = -\left(\tau_0 + \Delta\tau\cos\frac{2\pi t}{T}\right)\cos\frac{\pi(\theta-\theta_s)}{\theta_n-\theta_s} \tag{18b}$$

where θ is the latitude. The corresponding Ekman pumping rate is

$$w_{e,A} = \frac{1}{f\rho_0}\left[-\tau_0\left(\frac{\pi}{D}\sin\pi\theta' + \frac{\beta}{f}\cos\pi\theta'\right) + \Delta\tau\left(\frac{1}{D} - \frac{\beta}{f}\theta'\right)\cos\frac{2\pi t}{T}\right] \tag{19a}$$

$$w_{e,B} = \frac{1}{f\rho_0}\left[-\tau_0\left(\frac{\pi}{D}\sin\pi\theta' + \frac{\beta}{f}\cos\pi\theta'\right) - \Delta\tau\left(\frac{\pi}{D}\sin\pi\theta' + \frac{\beta}{f}\cos\pi\theta'\right)\cos\frac{2\pi t}{T}\right] \tag{19b}$$

where $D = 180/(r_0 \pi \Delta\theta)$ is a constant, r_0 is the radius of the Earth, $\Delta\theta = \theta_n - \theta_s$. We assume that thermocline depth along the eastern boundary is constant, the corresponding formulae are reduced to the following forms

$$h_I(0,y,t) = h_e - \frac{f^2}{\beta g' H}\int_0^{x_e} w_e\left(x, y, t - \frac{x}{C(y)}\right)dx \tag{20a}$$

$$\psi_I = -\frac{f}{\beta}\int_0^{x_e} w_e\left(x, y, t - \frac{x}{C(y)}\right)dx + \frac{1}{f\rho_0}\int_0^{x_e}\tau^x(x,y,t)\,dx \tag{20b}$$

$$h_W(0,y,t) = h_e - \frac{1}{\rho_0 g' H}\int_0^{x_e}\tau^x(x,y,t)\,dx \tag{20c}$$

As shown in Eq. (5), the speed of long Rossby waves depends on both the layer thickness and the Coriolis parameter. The main thermocline in the North Pacific Ocean is slightly shallower than that in the North Atlantic Ocean. In this study the mean thermocline depth in the Pacific-like (Atlantic-like) model ocean is set to 500 m (600 m). As a result, the speed of long Rossby waves in the Pacific-like model ocean is slightly slower than that in the Atlantic-like model, thin lines in Fig. 4. On the other hand, the Pacific-like model is twice as wide as the Atlantic-like model; thus, the basin-crossing time in the Pacific-like model is more than twice as that for the Atlantic-like model. In particular, the long Rossby waves take about 21.5 yr to cross the Pacific-like model basin at 40^{o}N; while the corresponding time is approximately 9 yr in the Atlantic-like model basin. Difference in the time delay has profound effect on the time evolution of thermocline depth and transport of the western boundary current, as will be shown shortly.

On the other hand, the meridional pressure gradient is not affected by the delay of the long Rossby waves, as discussed above.

We assume that wind stress is in the forms shown in Eqs. (18), where $\tau_0 = 0.1N/m^2$, $\Delta\tau = 0.04N/m^2$, and $T = 20$ yr is the period, Fig. 5. The time evolution of the corresponding Ekman pumping rate is shown in Fig. 6. As shown in these two figures, wind stress and Ekman pumping rate reach their maximum value in the middle of the period (Case A) and the beginning (end) of the period (Case B), respectively.

As discussed above, under our assumptions the meridional pressure gradient along the western wall depends on the instantaneous zonal wind stress only; thus, meridional pressure gradient along the western wall oscillates in the sinusoidal way, with a simple 20 yr period, Fig. 7. The meridional pressure gradient is positive for most latitudes, except for a very narrow band near the southern/northern boundary in Case A. For the wind stress patterns used in this study, the meridional pressure gradient reaches its maximum at the middle latitude of the model basin.

On the other hand, both the western boundary current transport and the thermocline depth include the contribution due to the delayed Ekman pumping. Since wind stress is assumed to be independent of *x*, the Ekman pumping rate can be reduced to the following form for Case A

$$w_{e,A} = \frac{\Delta\tau}{f\rho_0}\left(\frac{1}{D} - \frac{\beta}{f}\theta'\right)\cos\frac{2\pi t}{T} = -F(y)E(y)\cos\frac{2\pi t}{T}, F(y) = \frac{\Delta\tau\beta}{f^2\rho_0}, E(y) = \theta' - \frac{f}{D\beta} \quad (21)$$

where $E(y)$ is a factor of order one; thus the amplitude of the delay integral is determined by the factor $F(y)$. After simple manipulations, the delay integrals in Eqs. (20) can be carried out analytically.

$$\int_0^L \cos\frac{2\pi(t-x/C)}{T} = \frac{CT}{\pi}\sin\frac{\pi L}{TC}\cos\frac{2\pi(t-L/2C)}{T} \tag{22}$$

$$h_{I,A}(0,y,t) = h_e + AE(y)\cos\frac{2\pi\left[t-L/2C(y)\right]}{T}, \tag{23}$$

where

$$A = \frac{\Delta\tau C(y)T}{\rho_0 g'\pi H}\sin\frac{\pi L}{TC(y)}. \tag{24}$$

Since $E(y)$ is a factor of order one, the oscillation amplitude of thermocline depth along the outer edge of the western boundary current is determined by factor A, which depends on both the phase speed and the period of wind stress perturbations. Eq. (23) also includes the delay term, $L/2C(y)$. This delay time is equal to the half of the basin-crossing time at given latitude, which is shown in Fig. 4.

Because $\sin(\pi L/TC)$ has a value between -1 and 1, it is readily seen that for given parameters, such as wind stress perturbation $\Delta\tau$, reduced gravity g', mean layer thickness H, and phase speed $C(y)$, small period oscillation should give rise to small oscillation amplitude of the thermocline depth. As the period of wind stress oscillation increases, the corresponding amplitude of oscillation increases; however, as the period is

approaches infinite, the amplitude is bounded due to the combination of another factor $\sin(\pi L / TC)$.

The amplitude of oscillations in the thermocline depth is thus dependent on the phase speed and period of wind stress oscillations. Assume the wind stress perturbation is $\Delta\tau = 0.04N / m^2$, the amplitude factor A calculated for the Pacific-like and Atlantic-like model basin is shown in Fig. 8. It is readily seen that for wind stress oscillations with annual cycle or period of a few years, the thermocline depth oscillation amplitude is less than 10 meter. In particular, amplitude of thermocline depth oscillations is quite small at high latitudes. However, it is to remind the reader that the reduced gravity model is valid for the time scale on the order of the basin-crossing time; thus, left parts of each panel of Fig. 8 are not very accurate, and they are included for a qualitative argument only.

As the period is increased, the amplitude of the thermocline depth oscillations gradually increased. For the Pacific-like model, the amplitude can be on the order of 60 m at lower latitudes, Fig. 8. The corresponding amplitude in the Atlantic-like basin is smaller because the basin is relatively narrower.

The transport of the western boundary current consists of two terms. The first term on the right-hand side of Eq. (20b) involves the delayed integral of the Ekman pumping and the second term is a simple integration of the instantaneous wind stress, with no time delay. As discussed above the Ekman delay term strongly depends on the period of oscillation in wind stress. For wind stress oscillation of annual frequency or period of a few years, the contribution due to the delayed Ekman pumping integral is very

small. However, at low frequency the contribution due Ekman pumping oscillations may become much more important, especially for lower latitudes, Fig. 9a.

On the other hand, the second term is independent of the period of wind stress oscillations. For Case A, the wind stress perturbation amplitude is a linear function of the latitudes, so that the amplitude of transport oscillations due to the zonal wind stress contribution is a linear function of latitude, and it is independent of the wind stress oscillation period, Fig. 9b.

Our discussion below will be primarily focused on the cases with wind stress oscillates with period of 20 yr. The depth of the main thermocline along the outer edge of the western boundary oscillates in a similar way, as shown in Figs. 10, 11. The most important feature shown in the time evolution of the main thermocline depth is as follows. As discussed above, for decadal wind stress variability, the thermocline depth variation can be on the order of a few tens of meters, Figs. 10 and 11. The amplitude of oscillations in the thermocline depth is large along the southern boundary, but it is much reduced near the northern boundary. In particular, for Case B the amplitude of thermocline depth oscillation is on the order of 250 m in the southern part of the Pacific-like basin.

The maximum of the thermocline depth oscillation has a pronounced delay which increases with the latitude, shown in Figs. 10 and 11. The delay of the thermocline depth displayed in these figures is consistent with the simple relation described in Eq. (23).

The thermocline depth oscillations in the Atlantic-like model has similar features. The major difference between the Pacific-like model and the Atlantic-like model is that both the maximal depth and the amplitude of oscillation in the Atlantic-like basin are

much smaller than those in the Pacific-like model. This difference is due to the fact that the Pacific-like model is twice as wide as the Atlantic like model. As shown in Fig. 8, the amplitude of the thermocline depth oscillation in a narrow basin is smaller than that in a wide basin.

It is worthwhile to emphasize that the maximal depth of the main thermocline in the North Pacific Ocean is approximately 500-600 m; however, the corresponding maximum depth in the North Atlantic Ocean is approximately 800 m. The main reason responsible to this difference is that the North Pacific Ocean is covered by a layer of relatively fresh water, giving rise to stratification in the upper ocean which is much stronger than that in the North Atlantic Ocean, Huang (2010).

Transport of the western boundary current also shows oscillations similar to those of the thermocline depth. As shown in Eq. (20b), transport of the western boundary current is a sum of the contribution due to delayed Ekman pumping integral and the zonal wind stress integral. Both of these terms are simple sinusoidal functions in the present cases. The contribution due to delayed Ekman pumping is with a phase shift due to the delayed integral, the same as discussed in Eq. (23). The time evolution of the transport of the western boundary current in the Pacific-like model is shown in Figs. 12 and 13. Similar to the case of thermocline depth oscillations, the amplitude of oscillation is the largest in the southern part of the basin, while in the northern part of the basin, it is greatly diminished. There is clearly a phase shift which increases with latitude, and it is half of the basin-crossing time for the corresponding latitude.

As discussed in the previous section, transport of the western boundary current consists of contributions due to delayed Ekman pumping and the zonal wind stress integral. Although at interannual frequency contribution due to delayed Ekman pumping is relatively small, at decadal time scale the corresponding contribution can be quite large. In the present cases with a 20-year period oscillation in wind stress, the corresponding contribution due to delayed Ekman pumping (Fig. 14) is larger than the component due to zonal wind stress integral (Fig. 15).

The time evolution of western boundary current transport in the Atlantic-like model is similar; however, the amplitude of oscillations in these cases is smaller than that in the Pacific-like model basin (figures not included). This difference is primarily due to the fact that the basin-crossing time in the Atlantic-like model is half of that in the Pacific-like model. As shown in Fig. 8, the delayed integral of the Ekman pumping term is smaller in a narrow basin than in a wide basin.

For the wind stress pattern with decadal variability, the amplitude of perturbations in the depth of the thermocline at the outer edge of the western boundary and the transport of the western boundary current are quite large. However, as discussed in the previous section, for high frequency oscillations in wind stress, these two fields have quite different features.

3. A simple test of theory

To validate the simple theory postulated above, we calculated the wind stress integral and the layer thickness along the edge of the “western wall” in the North pacific

diagnosed from SODA data (http://ingrid.ldeo.columbia.edu/SOURCES/.CARTON-GIESE/SODA) , Carton and Giese (2008) in two station pairs P1 and P2 respectively, and the corresponding gradient between P1 and P2 are also given. The locations of P1 and P2 were chosen according to the mean thermocline depth defined by 14°C isotherm (Table 1).

Here, the layer thickness along the edge of the "western wall", h_W , is defined by and 14°C isotherm respectively. We emphasize that contributions due to zonal wind stress term ($-\int_0^{x_e} \frac{\partial \tau^x}{\partial y} dx$) and thermocline depth ($\frac{\partial h_w}{\partial y}$) are comparable under the assumption that the layer thickness along the eastern boundary, $h_e(x_e, y, t)$ in Eq. 16, is constant.

The climatological mean of the integral of wind stress and the thermocline depth are shown in Table 1. The meridional pressure force set up by the basin-scale wind stress along the wall is always northward in the subtropical gyre circulation. The layer thickness along the edge of the "western wall" diagnosed by SODA also decreases northward, which is consistent with the theory results.

Fig.16 shows the 2-8yr signals of the gradient between P1 and P2 estimated from SODA thermocline depth and the wind stress integral respectively. The zero-lag correlation coefficient between the diagnosed and theory results reaches 0.34 (> 95% confidence level) in station pair I and II (Fig. 17). In addition, the amplitude agreement is good. That is to say that, for category I and II, the interannual variability estimated by

theory and diagnosed results are both consistent, especially in 1963, 1972-1973, 1978-1980, 1983-1984, 1993-1995 and 2005-2006.

On the decadal time scale, the gradient between P1 and P2 in station I and II estimated by thermocline depth and wind stress integral are both consistent (Fig. 17). The zero-lag correlation coefficient between theory and diagnosed results reaches to 0.60 and 0.57 (> 95% confidence level) respectively. The above analysis shows that the theory is basically applicable on the longer time scale. This result provides a consistent support for the simple theory presented in this study.

4. Summary and discussion

In order to break the theoretical barrier between the open ocean circulation and the coastal circulation, we re-examined the classical reduced gravity model forced by variable wind stress. Since the reduced gravity model is valid for time scales longer than the cross-basin time of the first baroclinic Rossby waves, our model is not valid for seasonal time scale; however, it is applicable for interannual/interdecadal time scale. In addition, our model is aimed at the gyre-scale circulation and formulated without the inertial term, so that it cannot include the dynamical contribution due to meso-scale eddies produced by instability.

Most importantly, the meridional pressure gradient along the “western wall” of the model basin can be calculated as the meridional gradient of the zonal wind stress integrated from the western boundary to the eastern boundary, without the time delay associated with the propagation of the first baroclinic Rossby waves. On the other hand,

the transport of the western boundary current includes the contribution due to the zonal wind stress integral and the Ekman pumping subject to the time delay of the first baroclinic Rossby waves.

Therefore, the contributions to the coastal circulation adjacent to the western edge of the wind-driven gyre from these two terms can be treated as nearly independent from each other. The details of the corresponding physics will be discussed in Part II of this study.

Acknowledgement: This study was supported by the National Natural Science Foundation of China through Grant 40806005 and partially supported under the SCSIO Grant SQ200814. Drs. K. H. Brink and S. J. Lentz provided very useful comments on the early version of this manuscript.

References:

Brink, K.H., 1998: Deep-sea forcing and exchange processes. In *The Sea*, volume 10, K.H. Brink and A.R. Robinson, editors, J. Wiley & Sons, New York, 151-170.

Carton, J. A. and Giese, B. S. (2008): A reanalysis of ocean climate using Simple Ocean Data Assimilation (SODA). *Month. Wea. Rev*., **136**, 2999-3017.

Huang, R. X., 2010: *Ocean circulation, wind-driven and thermohaline processes*, Cambridge University Press, Cambridge, United Kingdom, 806 pp.

Hong, B.G., W. Sturges, and A. J. Clarke, 2000: Sea Level on the U.S. East Coast: Decadal Variability Caused by Open Ocean Wind-Curl Forcing. *J. Phys. Oceanogr*., **30**, 2088-2098.

Liu, Q.-Y. and R. X. Huang: Meridional circulation in the western coastal zone, Part II. The regulation by pressure gradient set up through basin scale circulation and the western boundary current transport, manuscript submitted to *J. Phys. Oceanogr*.

Qiu, B., 2002; Large-Scale Variability in the Midlatitude Subtropical and Subpolar North Pacific Ocean: Observations and Causes *J. Phys. Oceanogr.,* **32,** 353–375.

Schlichting, H., 1979: *Boundary layer theory*, McGraw-Hill, New York, 817pp.

Willebrand, J., S. G. H. Philander, and R. C. Pacanowski, 1980: The oceanic response to large-scale atmospheric disturbances. *J. Phys. Oceanogr.,* **10,** 411–429.

Yang, J.-Y., 2007: An Oceanic Current against the Wind: How Does Taiwan Island Steer Warm Water into the East China Sea? *J. Phys. Oceanogr*., **37**, 2563-2569.

Figure captions:

Fig. 1**:** The framework of the ocean, which is separated into three parts, the interior flow, the western boundary layer current, and the costal current over the continental shelf. The coastal circulation here is treated as a thin boundary layer attached to the interior solution and the western boundary current. The continental slope is very steep; as an approximation it is treated as a vertical wall in this study.

Fig. 2. Volumetric transport balance for a zonal section, including the Ekman layer, subsurface layer in the ocean inteior, and the western boundary current.

Fig. 3**.** A numeical example of thermoclien depth (left panel) and free surface elevation (right panel) in a two-gyre basin.

Fig. 4. Speed of the long Rossby waves and the basin-crossing time for: a) the Pacific basin (120^o wide); b) the Atlantic basin (60^o wide).

Fig. 5. Wind stress applied to a subtropical basin, oscillating with a 20 year period.

Fig. 6. Ekman pumping velocity.

Fig. 7. Meridional pressure gradient along the western wall: a) distribution over the whole length of the western wall; b) time series of pressure gradient along selected latitud

Fig. 8. Amplitude of oscillations in the thermocline depth.

Fig. 9. Amplitude of oscillations in the western boundary current transport due to contribution from the Ekman pumping term (left panel) and the zonal wind stress (right panel) for Case A.

Fig. 10. Time evoloution of the thermocline depth along the outer edge of the westenr boundary current in the Pacific-like model under wind stress with oscillations of 20-year period.

Fig. 11. Time evolution of the thermocline depth along the outer edge of the western boundary current in the Pacific-like model under wind stress which oscillates with 20-year period, at four stations along the western boundary.

Fig. 12. Time evoloution of the transport of the westenr boundary current in the Pacific-like model under wind stress with oscillations of 20-year period.

Fig. 13. Tranport at different sections for the Pacific-like model.

Fig. 14. Time evoloution of the wind stress component of the transport of the western boundary current in the Pacific-like model under wind stress with oscillations of 20-year period.

Fig. 15. Time evoloution of the Ekman pumping component of the transport of the westenr boundary current in the Pacific-like model under wind stress with oscillations of 20-year period.

Fig.16. The standarized interannual variability of the gradient of the wind stress integral and the thermocline depth diagnosed by SODA between P1 and P2. A bandpass filter is used to extract the 2-8yr signals.

Fig.17. The standarized interdecdal variability (>10yr) of the gradient of the wind stress integral and the thermocline depth diagnosed by SODA between P1 and P2.

Table and Figures:

Table 1: The locations of P1 and P2 and the related climatology mean of the wind stress integral and the thermocline depth defined by 14^{o}C isotherm diagnosed by SODA.

Location of the station pair		Wind Stress Integral (N/m)	Thermocline Depth (m)
I	P1 (121.75E,22.75N)	6.31×10^{5}	263
	P2 (121.75E, 23.75N)	5.52×10^{5}	186
II	P1 (121.25E, 22.75N)	6.33×10^{5}	215
	P2 (121.75E, 23.75N)	5.52×10^{5}	186

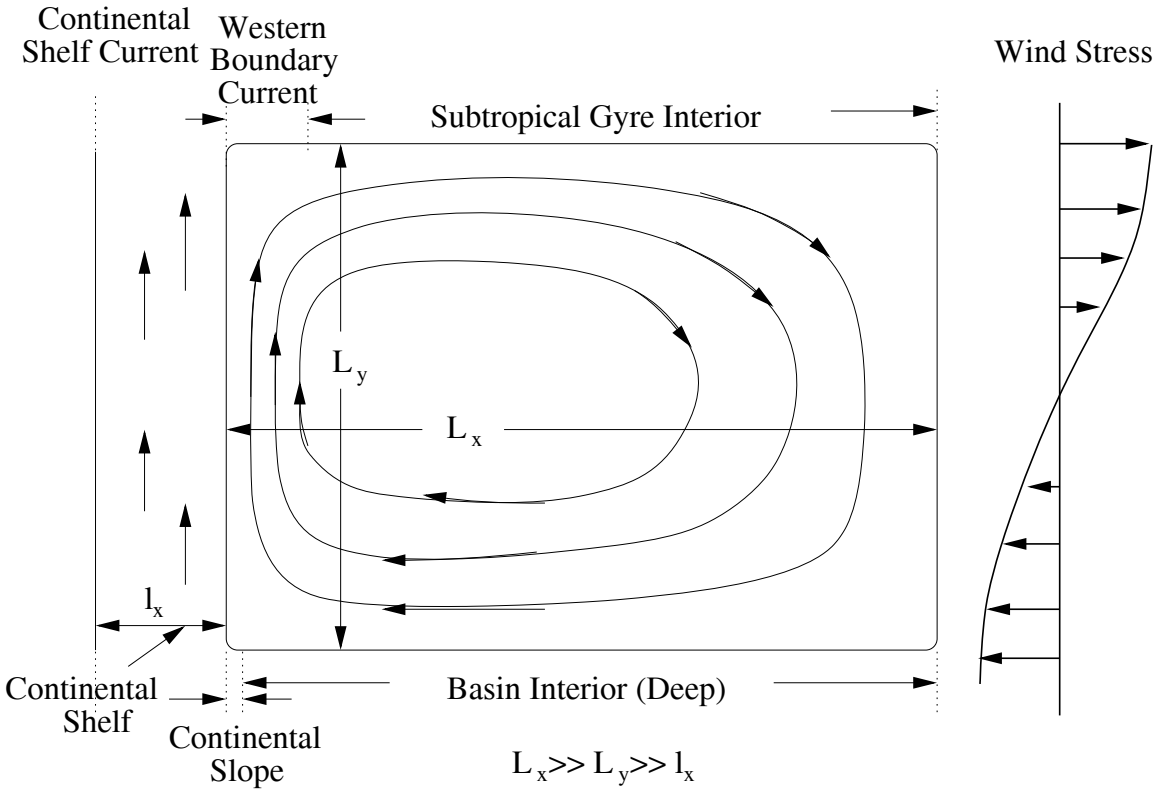

Fig. 1**:** The framework of the ocean, which is separated into three parts, the interior flow, the western boundary layer current, and the costal current over the continental shelf. The coastal circulation here is treated as a thin boundary layer attached to the interior solution and the western boundary current. The continental slope is very steep; as an approximation it is treated as a vertical wall in this study.

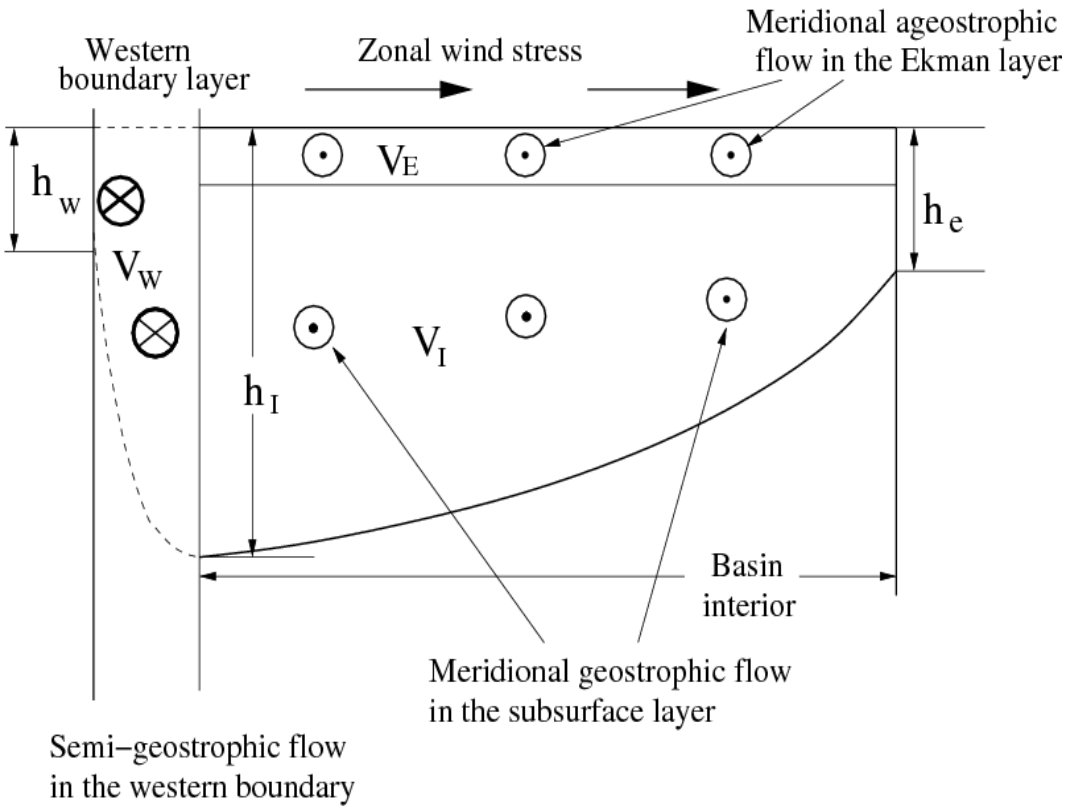

Fig. 2. Volumetric transport balance for a zonal section, including the Ekman layer, subsurface layer in the ocean inteior, and the western boundary current.

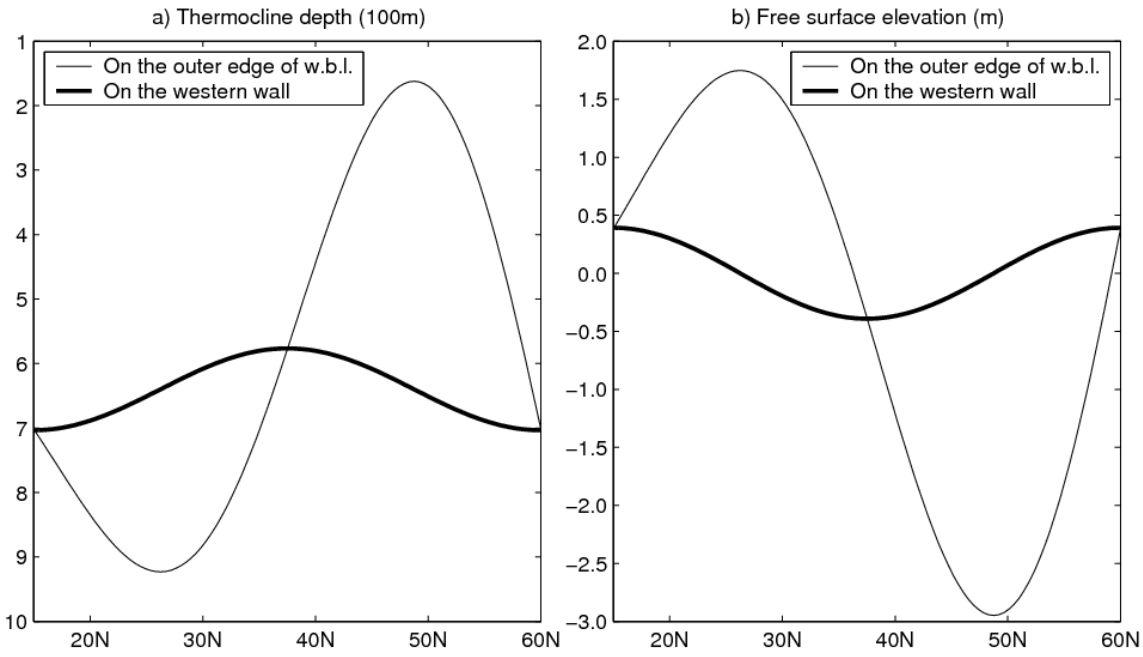

Fig. 3**.** A numeical example of thermoclien depth (left panel) and free surface elevation (right panel) in a two-gyre basin.

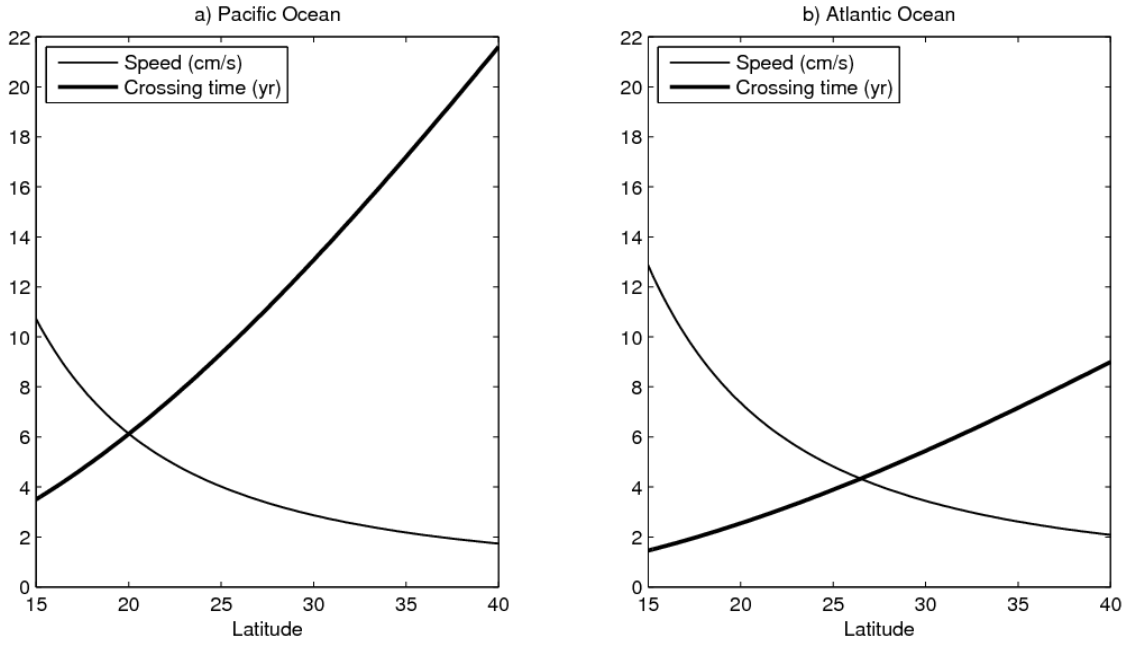

Fig. 4. Speed of the long Rossby waves and the basin-crossing time for: a) the Pacific basin (120^o wide); b) the Atlantic basin (60^o wide).

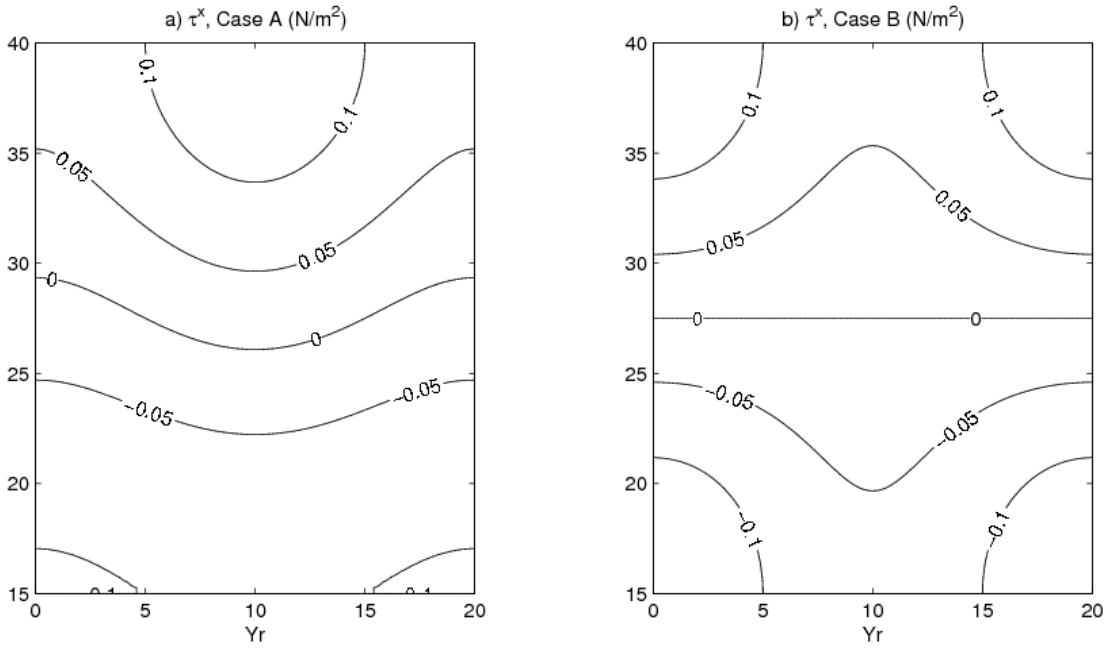

Fig. 5. Wind stress applied to a subtropical basin, oscillating with a 20 year period.

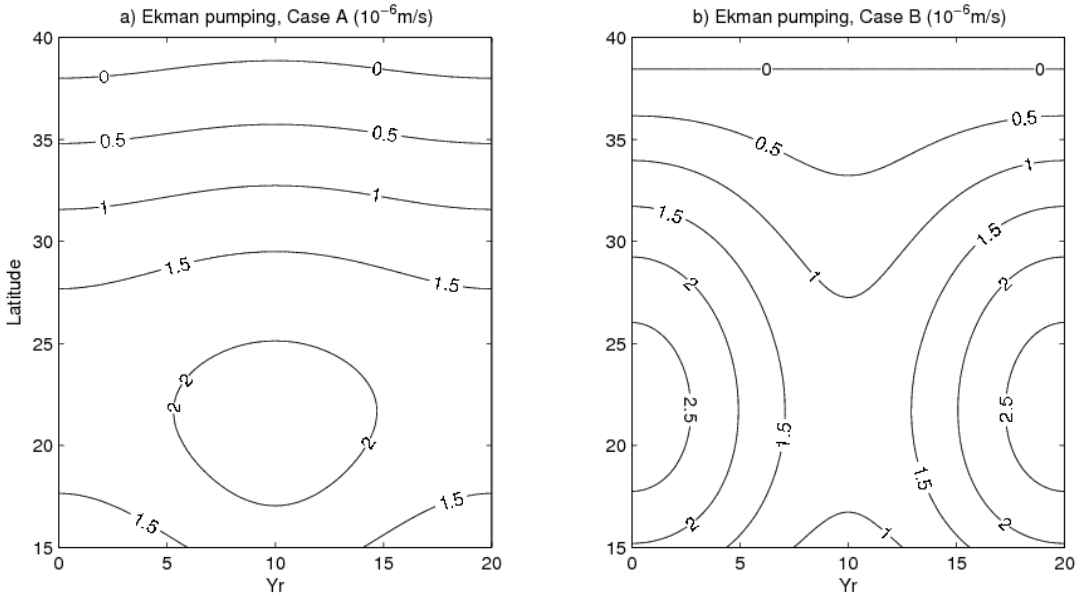

Fig. 6. Ekman pumping velocity.

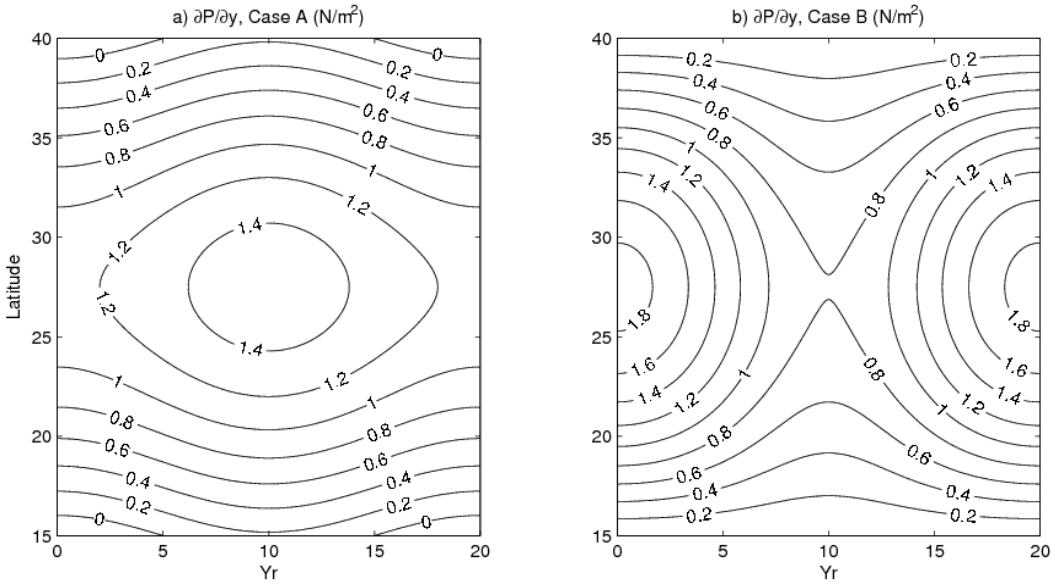

Fig. 7. Meridional pressure gradient along the western wall: a) distribution over the whole length of the western wall; b) time series of pressure gradient along selected latitude locations.

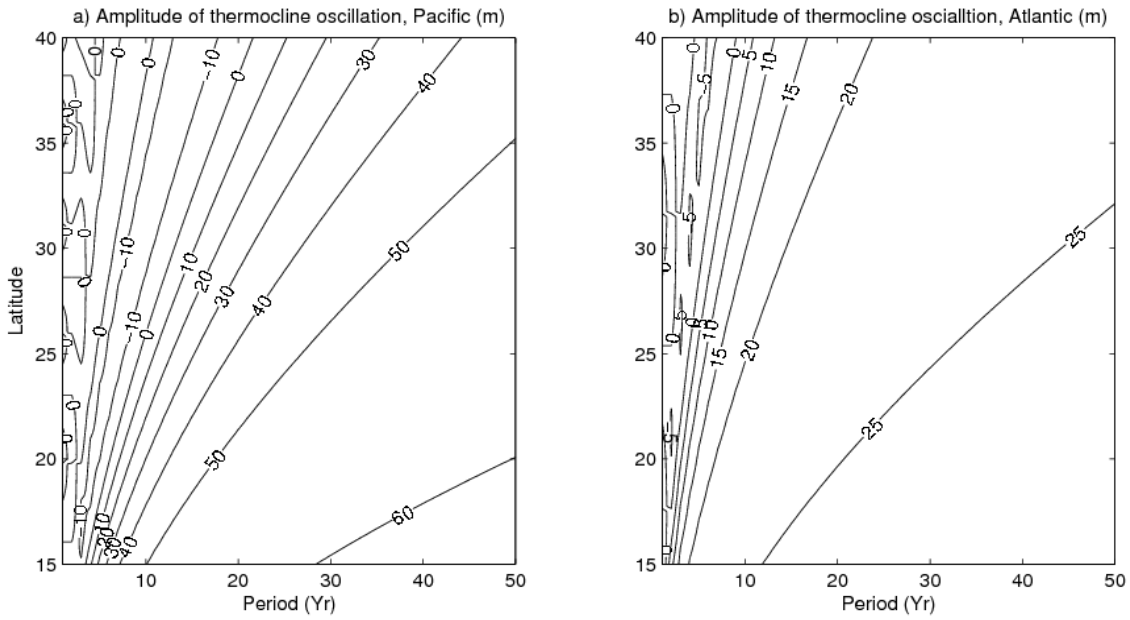

Fig. 8. Amplitude of oscillations in the thermocline depth.

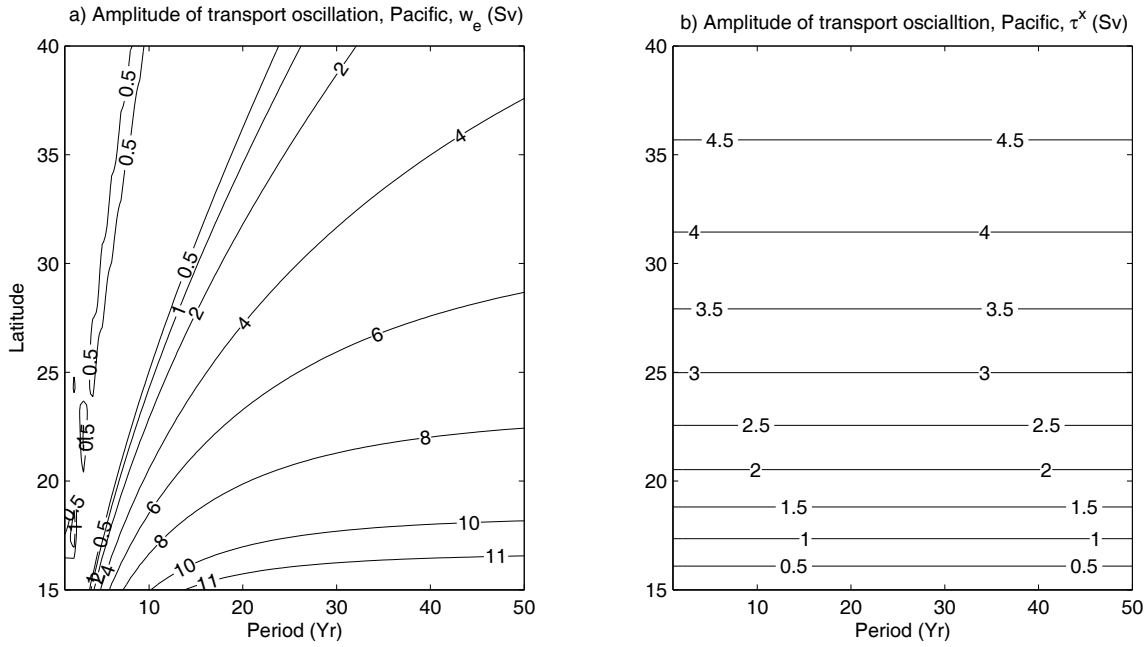

Fig. 9. Amplitude of oscillations in the western boundary current transport due to contribution from the Ekman pumping term (left panel) and the zonal wind stress (right panel) for Case A.

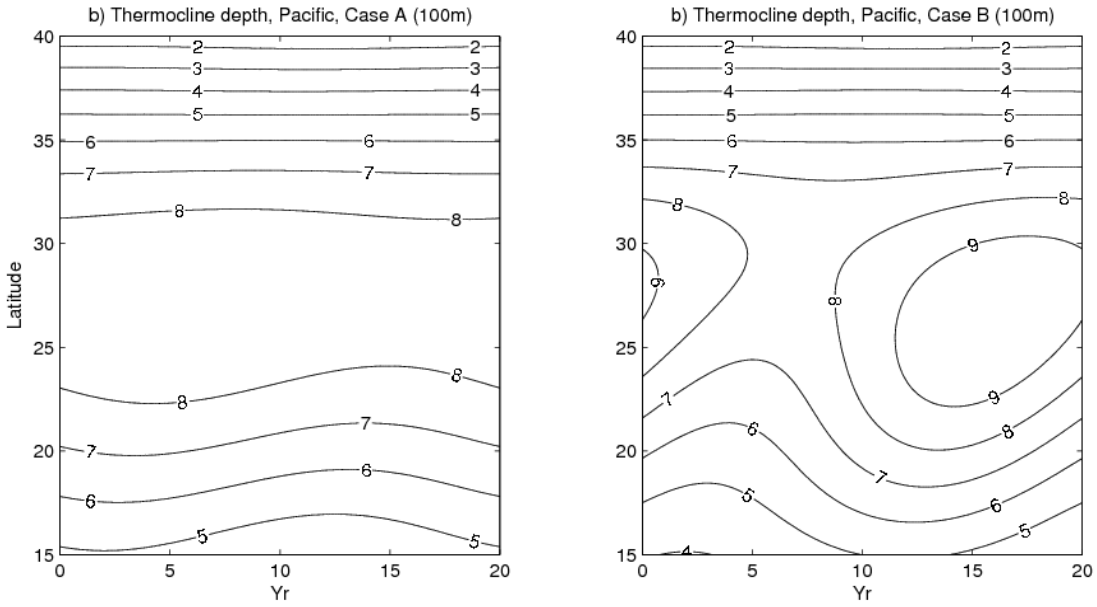

Fig. 10. Time evoloution of the thermocline depth along the outer edge of the westenr boundary current in the Pacific-like model under wind stress with oscillations of 20-year period.

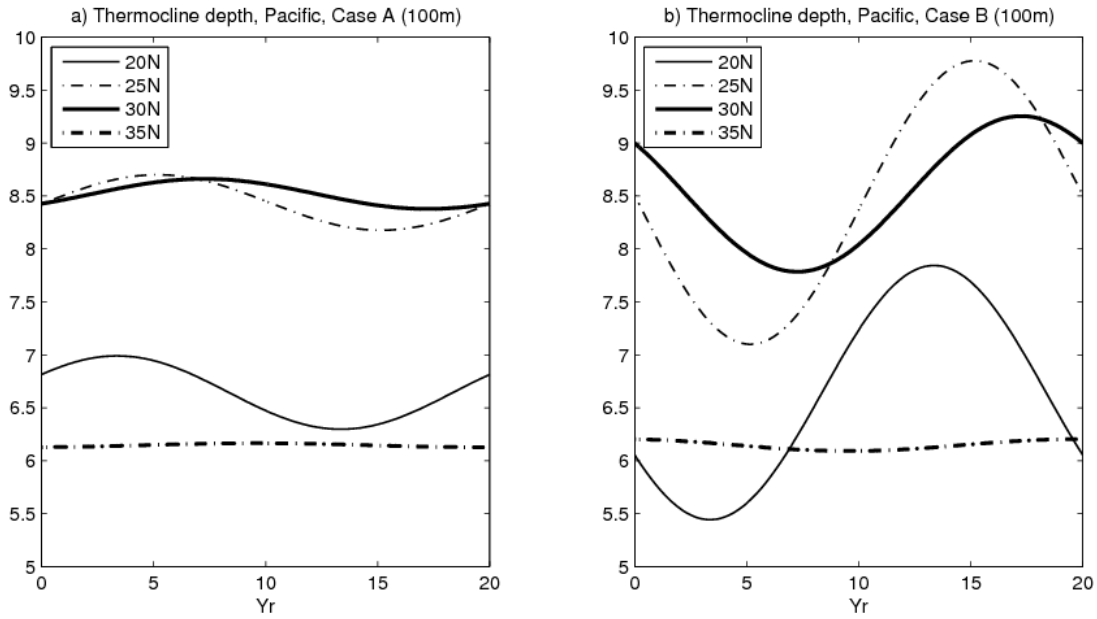

Fig. 11. Time evolution of the thermocline depth along the outer edge of the western boundary current in the Pacific-like model under wind stress which oscillates with 20-year period, at four stations along the western boundary.

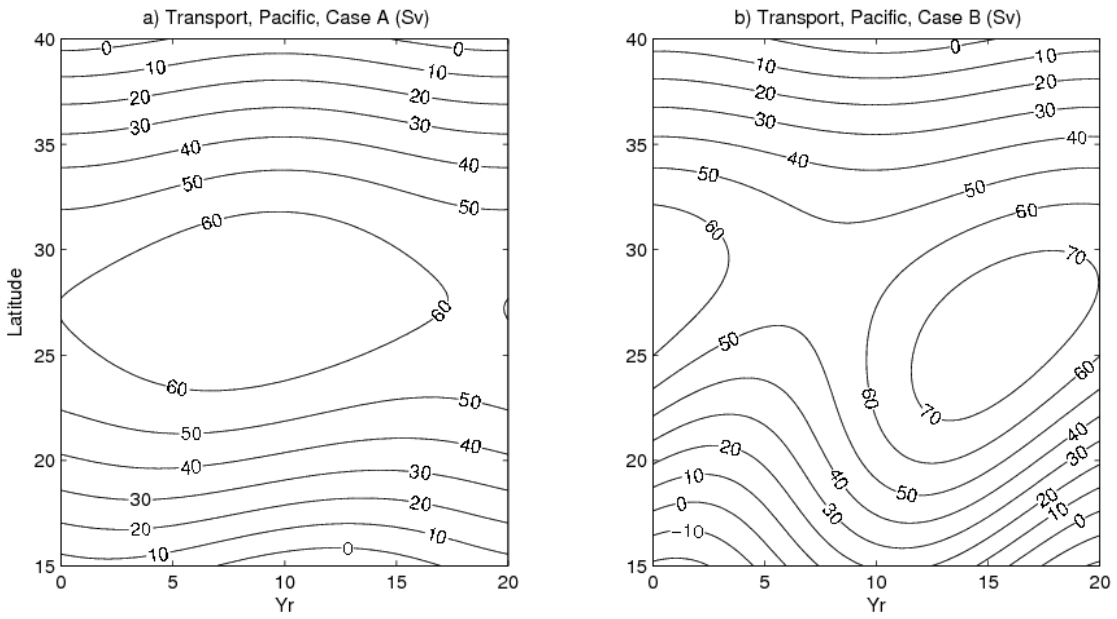

Fig. 12. Time evoloution of the transport of the westenr boundary current in the Pacific-like model under wind stress with oscillations of 20-year period.

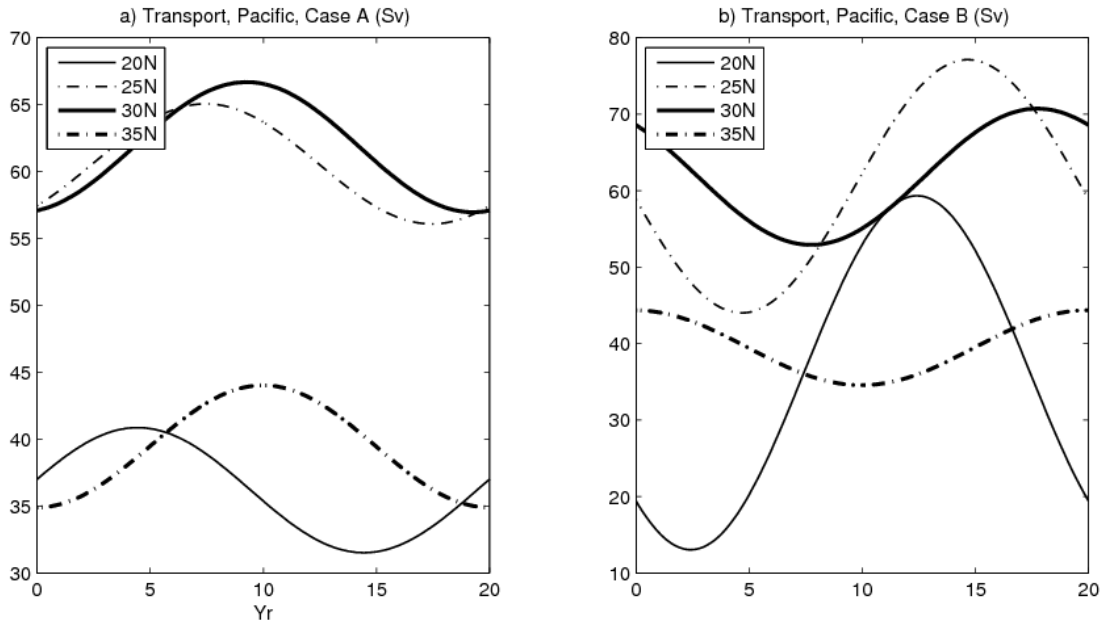

Fig. 13. Tranport at different sections for the Pacific-like model.

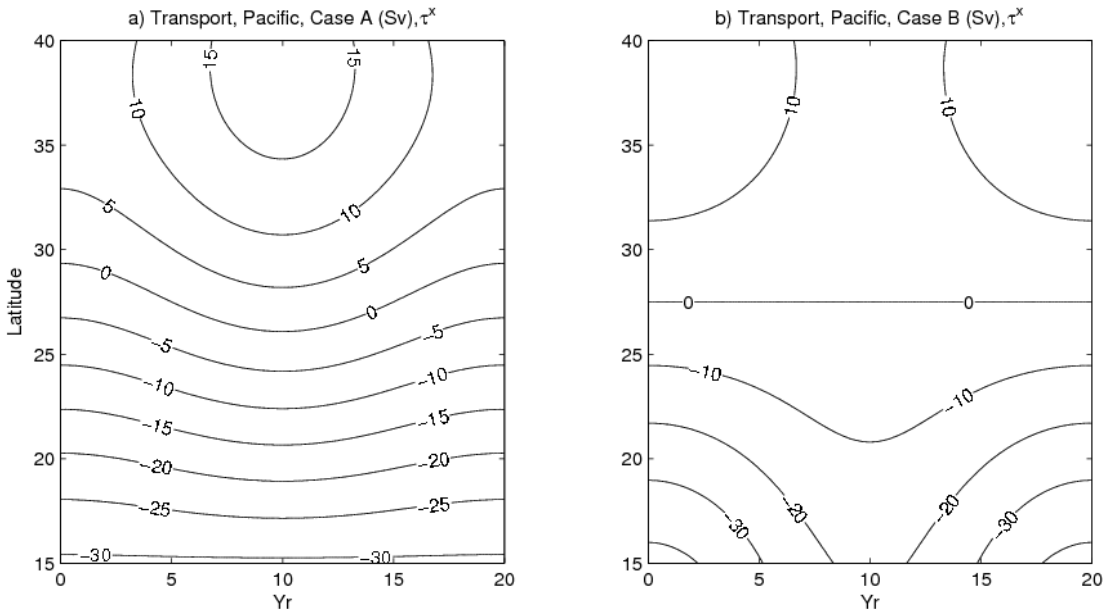

Fig. 14. Time evoloution of the wind stress component of the transport of the western boundary current in the Pacific-like model under wind stress with oscillations of 20-year period.

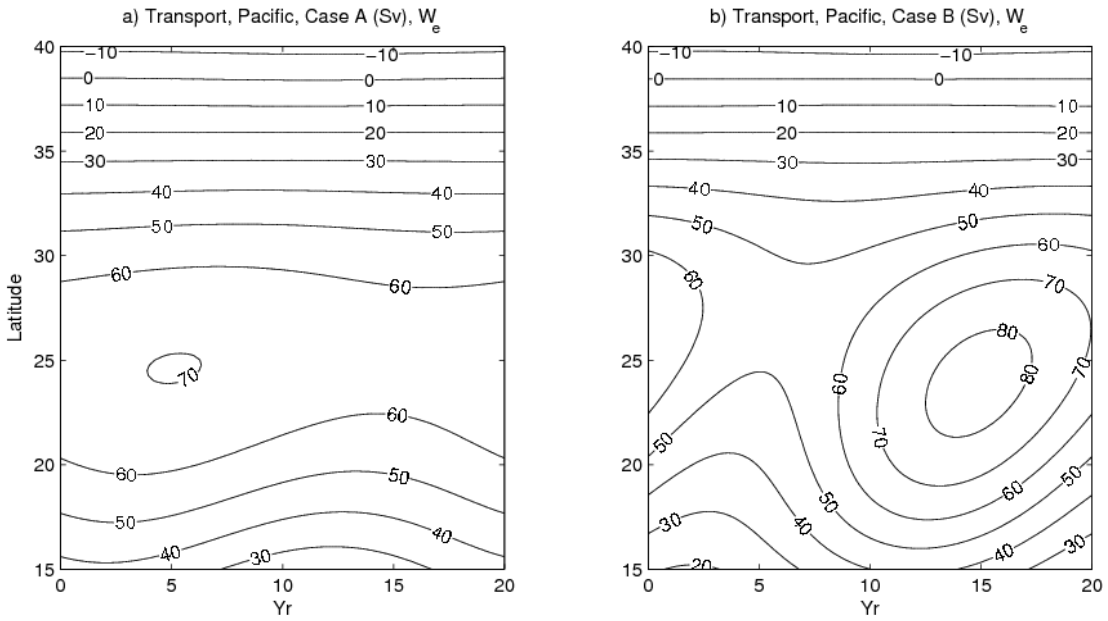

Fig. 15. Time evoloution of the Ekman pumping component of the transport of the westenr boundary current in the Pacific-like model under wind stress with oscillations of 20-year period.

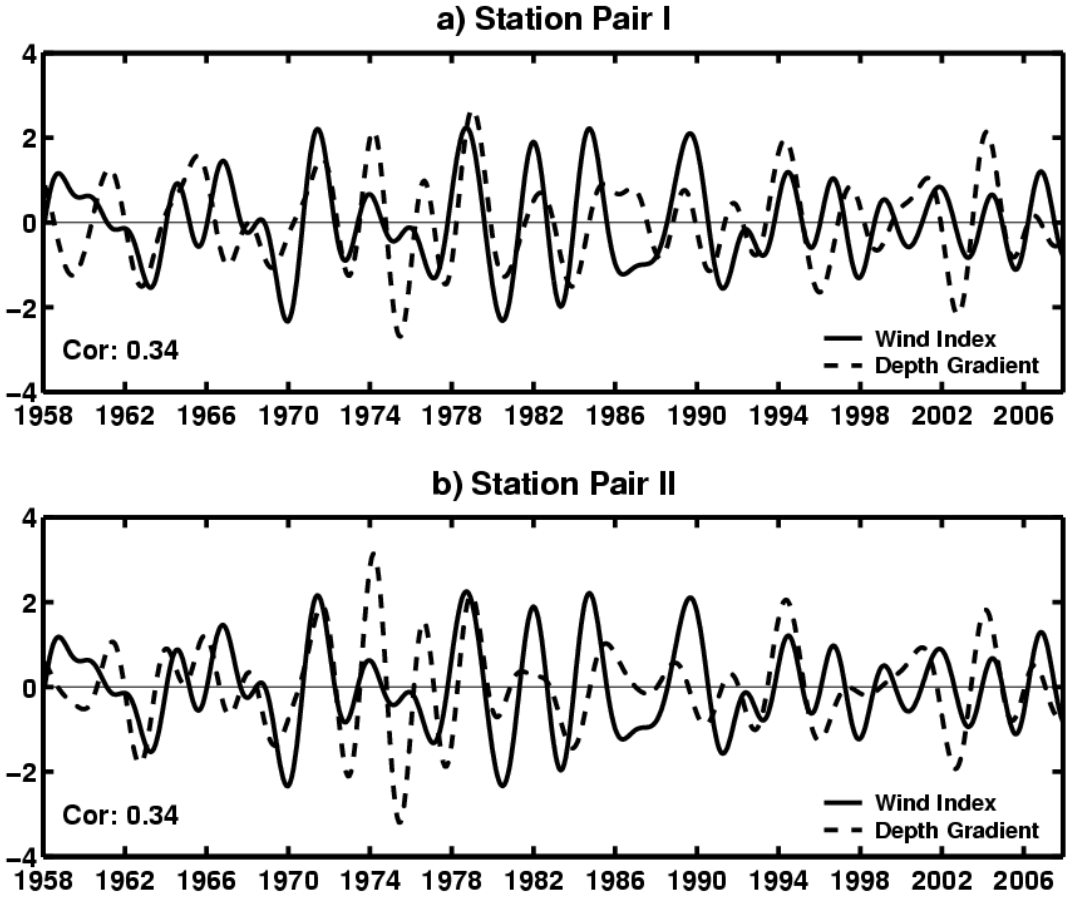

Fig.16. The standarized interannual variability of the gradient of the wind stress integral and the thermocline depth diagnosed by SODA between P1 and P2. A bandpass filter is used to extract the 2-8yr signals.

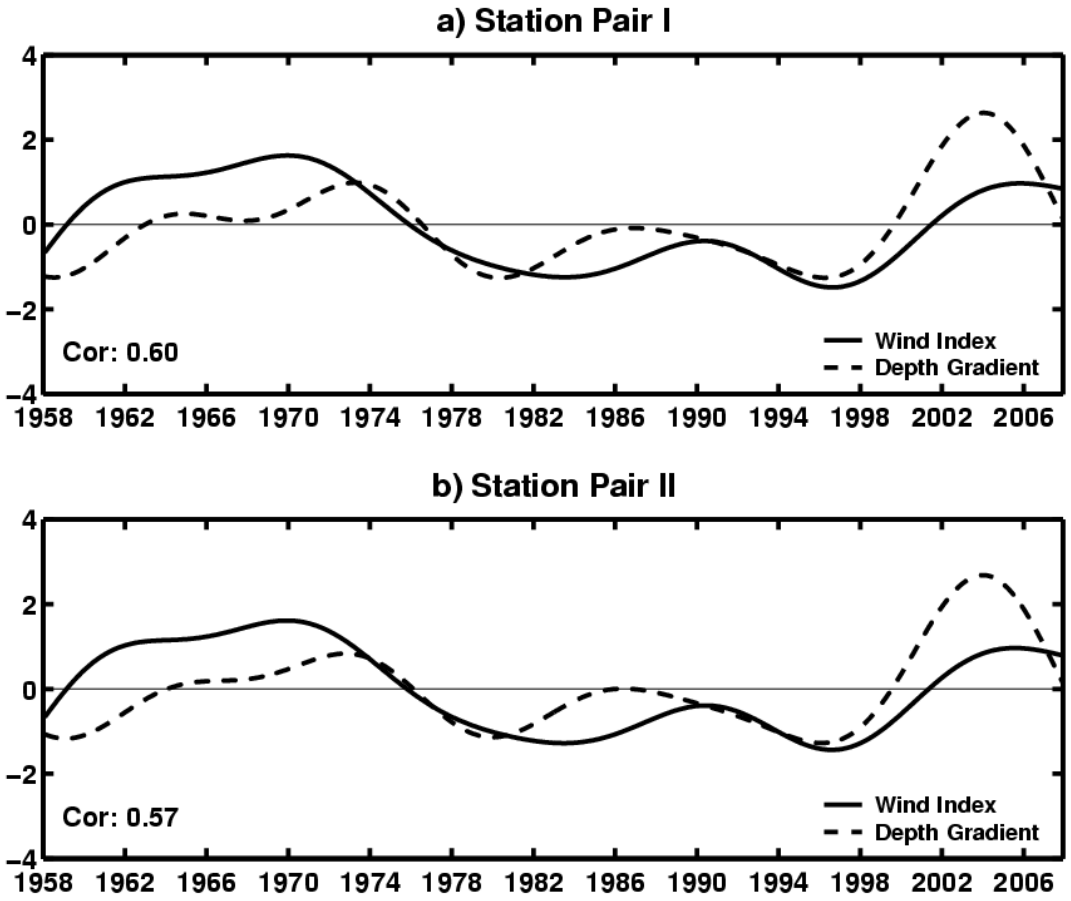

Fig.17. The standarized interdecdal variability (>10yr) of the gradient of the wind stress integral and the thermocline depth diagnosed by SODA between P1 and P2.